

Ax-BxP: Approximate Blocked Computation for Precision-Reconfigurable Deep Neural Network Acceleration

Reena Elangovan¹, Shubham Jain², Anand Raghunathan¹

¹School of Electrical and Computer Engineering, Purdue University

²IBM T.J. Watson Research Center, Yorktown Heights, NY

{elangovr, raghunathan}@purdue.edu, shubham.jain35@ibm.com

Abstract—Precision scaling has emerged as a popular technique to optimize the compute and storage requirements of Deep Neural Networks (DNNs). Efforts toward creating ultra-low-precision (sub-8-bit) DNNs suggest that the minimum precision required to achieve a given network-level accuracy varies considerably across networks, and even across layers within a network, requiring support for variable precision in DNN hardware. Previous proposals such as bit-serial hardware incur high overheads, significantly diminishing the benefits of lower precision. To efficiently support precision re-configurability in DNN accelerators, we introduce an approximate computing method wherein DNN computations are performed block-wise (a block is a group of bits) and re-configurability is supported at the granularity of blocks. Results of block-wise computations are composed in an approximate manner to enable efficient re-configurability. We design a DNN accelerator that embodies approximate blocked computation and propose a method to determine a suitable approximation configuration for a given DNN. By varying the approximation configurations across DNNs, we achieve 1.11x-1.34x and 1.29x-1.6x improvement in system energy and performance respectively, over an 8-bit fixed-point (Fxp8) baseline, with negligible loss in classification accuracy. Further, by varying the approximation configurations across layers and data-structures within DNNs, we achieve 1.14x-1.67x and 1.31x-1.93x improvement in system energy and performance respectively, with negligible accuracy loss.

I. INTRODUCTION

Deep Neural Networks (DNNs) have become very popular in recent years due to their ability to achieve superhuman performance in a variety of cognitive tasks such as image classification, speech recognition and natural language processing [1], [2], [3]. The remarkable algorithmic performance of DNNs comes with extremely high computation and storage requirements. While these challenges span both training and inference, we focus on the latter scenario where the high computation requirements of DNNs limit their adoption in energy- and cost-constrained devices [4].

The use of low precision has emerged as a popular technique for realizing DNN inference efficiently in hardware [5], [6]. Low precision or bit-width favorably impacts all facets of energy consumption including computation, interconnect, and memory. State-of-the-art commercial DNN hardware widely

supports 8-bit precision for DNN inference, and recent research continues to explore techniques to push towards even lower precision [7], [8], [9], [10], [11].

Recent efforts [7], [12], [13] suggest that realizing ultra-low-precision (sub-8-bit) DNN inference without any accuracy degradation is quite challenging if the precision for all data-structures is scaled uniformly. Therefore, the use of variable precision across DNNs, and across layers within a DNN, has gained considerable interest. For instance, HAQ[7] shows that the MobileNet and ResNet DNNs require precision varying from 3 to 8 bits across network layers in order to match the accuracy of a full-precision network.

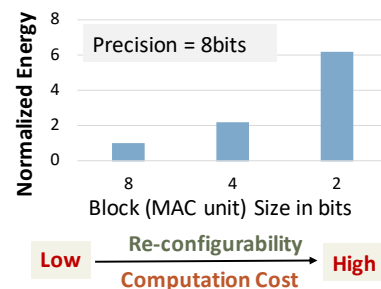


Fig. 1: Computation cost vs re-configurability trade-offs

To support variable precision, one option is to utilize conventional fixed-precision hardware that is provisioned for the worst case precision, possibly gating the unused portions of logic to save power. However, such a design does not fully utilize the potential of aggressive precision-scaling. Alternatively, variable-precision DNN accelerators with bit-serial [14], [15], [16] or bit-fused [17] fabrics have been designed to support re-configurability. However, this re-configurability comes at a high cost as the bit-serial arithmetic circuits incur significant energy and latency overheads with respect to their fixed-precision counterparts of equivalent bit-width, due to multi-cycle operation and control logic. Figure 1 quantifies the energy overhead (at iso-area) incurred while performing 8-bit MAC computations using digit-serial hardware (MAC units) of 2-bits and 4-bits (synthesized to 15nm with Synopsys Design Compiler). As shown, the increased flexibility provided by smaller blocks is accompanied by a much higher energy cost for 8-bit arithmetic. This limits the energy benefits that can be realized from variable-precision DNNs, wherein the minimum

bit-width varies between 2-8 bits across layers and across networks [7], [12], [13].

To design hardware for DNNs that caters to variable precision requirements with minimal overheads, we leverage the intrinsic tolerance of DNNs to approximate computation, which is the basis for reduced precision itself [13]. We introduce an approximate computation method to execute DNN inference in which weights and activations are composed of fixed-length blocks (groups of bits), and computations are performed block-wise. Approximate composition of results across blocks is utilized to enable efficient re-configurability at the block granularity. We present a methodology to perform inference by choosing the best approximation configuration for each layer. We also propose architectural enhancements to realize Approx-BxP in a standard systolic array based DNN inference accelerator with minimal design modifications. We show that (i) Approx-BxP with varying approximation configurations across DNNs achieves 1.11x-1.34x and 1.29x-1.6x improvement in system-level energy and performance respectively, and (ii) Approx-BxP with varying approximation configurations across layers within DNNs obtains 1.14x-1.67x and 1.31x-1.93x improvement in system-level energy and performance respectively, in both cases with negligible loss ($\leq 1\%$) in classification accuracy with respect to an 8-bit fixed-precision (Fxp) baseline.

II. PRELIMINARIES

A. Blocked Fixed Point

Fixed-point (Fxp) format is widely used for efficient realization of low-precision DNNs. Blocked fixed-point (Bxp) format is an adaptation of the Fxp format where the data bits are partitioned into fixed length blocks. In particular, an $(N * K)$ bit signed Fxp number X_{Fxp} can be represented as a Bxp number X_{Bxp} with N blocks, each of K bits as shown in Figure 2(a). The blocks of X_{Bxp} are arranged in the decreasing order of significance (place value) by default, where the significance of the i^{th} block X_i is 2^{i*K} . Here, the most significant block X_{N-1} is a signed block. The magnitude of X_{Bxp} denoted $|X_{Bxp}|$, can be derived from its blocks as shown in the figure.

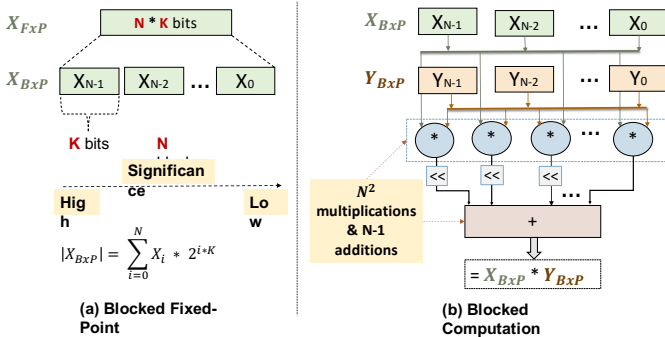


Fig. 2: Bxp: Overview

B. Blocked Multiplication

Figure 2(b) demonstrates a blocked¹ multiplications between two Bxp format numbers X_{Bxp} and Y_{Bxp} . As shown, each block of X_{Bxp} is multiplied with each block of Y_{Bxp} to generate N^2 partial products (P). Subsequently, partial products are shifted and accumulated using $N^2 - 1$ additions. Equation 1 expresses an exact blocked multiplication operation, where P_{ij} [$P_{ij} = X_i * Y_j$] represents the partial product of the i^{th} (X_i) and j^{th} (Y_j) block of X_{Bxp} and Y_{Bxp} , respectively.

$$X_{Bxp} * Y_{Bxp} = \sum_{i=0}^{N-1} \sum_{j=0}^{N-1} P_{ij} * 2^{(i+j)*K} \quad (1)$$

III. APPROXIMATE BLOCKED COMPUTATION

In this section, we discuss Ax-Bxp, *i.e.*, our proposed approximate blocked computation method for designing efficient precision-reconfigurable DNNs. We first detail the key approximation concepts and introduce Ax-Bxp format for representing MAC operands. Subsequently, we present a systematic methodology for designing Ax-Bxp without compromising application-level accuracy. Finally, we demonstrate the integration of Ax-Bxp into a standard systolic array-based DNN accelerator using simple hardware extensions.

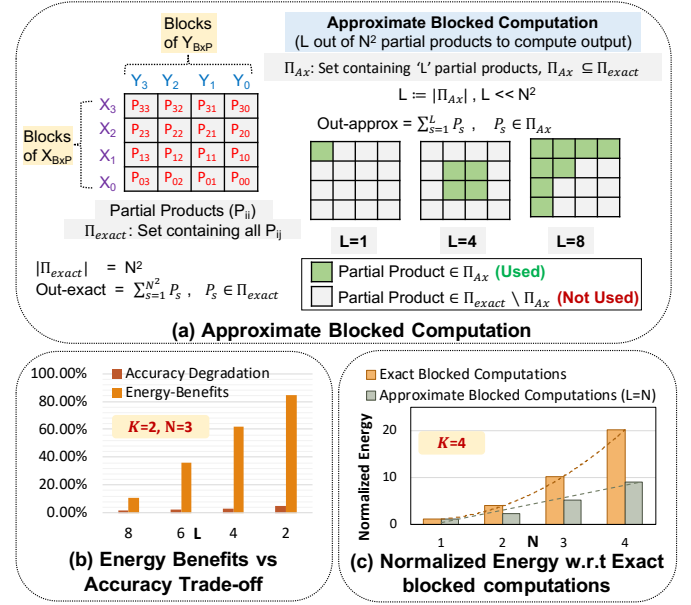


Fig. 3: Approximate blocked computation: Overview

A. Approximation Method

The main idea in Ax-Bxp is to perform blocked computations by selecting a subset of partial products (out of the total N^2). Figure 3(a) illustrates the concept, where the multiplication of operands (X_{Bxp} and Y_{Bxp}) is performed by computing and accumulating only $L := |\Pi_{Ax}|$ out of

¹Blocked multiplication is also known in the literature as digit serial multiplication (e.g., [18]) and bit-level composable multiplication (e.g., [17]).

N^2 possible partial product terms. Formally (as shown in Figure 3(a)), we characterize Ax-BxP multiplication using a set $\Pi_{Ax} \subseteq \Pi_{Exact}$, wherein the final output (out-approx) is given by summing the partial products (P_s) in Π_{Ax} . Ax-BxP has two design parameters — (i) L (the size of set Π_{Ax}) and (ii) the choice of elements (partial products) within the set Π_{Ax} . Both these design parameters affects the computational errors and the energy benefits, and thereby are explored to maximize energy-accuracy trade-offs. Next, we overview the design considerations involved in choosing L , and elements within the set (Π_{Ax}) for a given L .

Figure 3(b) presents the dis-proportional energy-accuracy benefits of Ax-BxP in the context of DNNs, across various choices of L with fixed values of N and K (i.e., $K = 2, N = 3$). As L decreases, the computational accuracy decreases minimally, whereas the energy benefits increase drastically. The dis-proportional energy-accuracy trade-off arises due to the typical data distribution seen in DNNs [11], wherein a majority (>90%) of the data elements are small and can be computed accurately at low-precision. To estimate energy benefits with respect to an exact computation, we synthesized the PEs (multipliers and adders) at 15nm technology node using Synopsys Design Compiler. The reported computational accuracy is for the best Π_{Ax} among all choices of Π_{Ax} . We also evaluated the energy benefit across various values of N by fixing the values of K and L ($K=4, L=N$). As shown in Figure 3(c), the energy of approximate block-wise computations increase linearly with N as we require $O(N)$ multiplications and additions. In contrast, energy of exact blocked computations increases quadratically as they require $O(N^2)$ computations.

For a given L , when fewer than N blocks of X_{BxP} or Y_{BxP} (or both) are used to construct Π_{Ax} , we can achieve memory footprint savings in addition to computation savings by storing only the required blocks. To leverage this, we introduce a new format for storing the Ax-BxP operands in the following subsection. Section III-C describes the *significance-* and *value-based* methods that we use for choosing the required blocks of the operands.

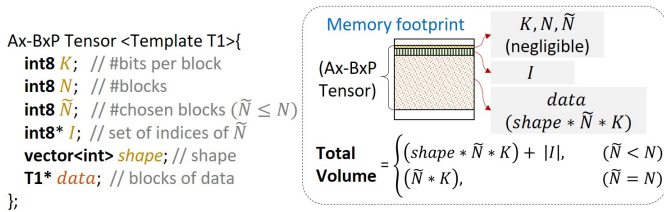


Fig. 4: Ax-BxP Tensor: Memory Layout

B. Ax-BxP Tensor

We introduce a new format for storing Ax-BxP operand blocks and their indices. Ax-BxP format uses the following fields – (i) total number of blocks (N), (ii) block-size (K), (iii) the set \mathcal{I} containing indices of the operand blocks chosen for Ax-BxP computation, (iv) number of chosen blocks ($\tilde{N} := |\mathcal{I}| \leq N$) and (v) data elements (*data*), wherein the data blocks are arranged in decreasing order of significance.

The size of the *data* is $\tilde{N} * K$ bits. Note that, during exact blocked computation, $\tilde{N} = N$ and \mathcal{I} is not required.

We define Ax-BxP Tensor as a tensor (typically the weights or activations of an entire layer) composed of scalar elements in the Ax-BxP Format, where the elements share a common meta-data (*viz.*, $N, K, \tilde{N}, \mathcal{I}$). Ax-BxP Tensor is presented as a template class in Figure 4, which also illustrates the memory layout of the different fields. Since the meta-data are amortized across an entire tensor, the associated memory footprint is negligible. Furthermore, compared to the case of $\tilde{N} = N$, when $\tilde{N} < N$ the size of the *data* field is small, resulting in savings in memory footprint and memory traffic in addition to computation.

C. Design Methodology

Next, we present key design considerations involved in approximating DNNs using Ax-BxP and the methodology we use to select the Ax-BxP format for each layer in the network. In this subsection, we first characterize the Ax-BxP design space. Subsequently, we provide pruning techniques to reduce the complexity of the design space exploration and algorithms for systematically designing Ax-BxP DNNs.

1) *Design Space Characterization*: For a given bit-width (BW), where $BW = N * K$, an Ax-BxP MAC operation (characterized by the set Π_{Ax}) can be designed in numerous ways. We define Ω as a set enumerating all possible ways of constructing Π_{Ax} . Equation 2 expresses the size of Ω ($|\Omega|$) which is determined by free variables L and N . As shown, for a given BW, we are free to choose N (i.e., number of blocks) to be an integer from 1 to BW. Subsequently, we can select the approximation-level by determining L , i.e., number of partial products to be used during MAC operations. The value of L can be 1 to N^2 , where $L=N^2$ represents an exact blocked computation. Lastly, there are $\binom{N^2}{L}$ ways of selecting L out of N^2 partial products.

$$|\Omega| = \sum_{N=1}^{BW} \sum_{L=1}^{N^2} \binom{N^2}{L} \quad (2)$$

2) *Design Space Constraints*: To reduce the search space $|\Omega|$ which is exponential in N , we put forth the following arguments to bound $|\Omega|$ by constraining BW, K , N , and L :

- *Bitwidth (BW)*: Since a bit-width of 8 for both activations and weights is sufficient to preserve accuracy during inference [19], we constraint $BW \leq 8$.
- *Bits in a block (K)*: We also bound K such that $1 < K \leq 4$. By setting $K > 1$, we avoid the latency and energy overheads associated with bit-serial ($K=1$) implementation [17]. Moreover, we introduce an upper-bound on K ($K \leq 4$) to avoid $N = 1$ (i.e., an FxP implementation).
- *Number of Blocks (N)*: We set N as $N = \lceil BW/K \rceil$. Therefore, for $BW \leq 8$ and $1 < K \leq 4$, the allowed values of N are 2,3 and 4.
- *Size of set Π_{Ax} (L)*: Lastly, we constraint $L \leq N$ based on the energy-accuracy trade-offs discussed in Section III-A and shown in Figure 3. We found that $L \leq N$ provides

ample design choices, wherein we can obtain significant energy benefits with minimal impact on computational accuracy. Apart from reduction in design space, bounding $L \leq N$ also helps in minimizing the design complexity of both the control logic and Ax-BxP PEs at core-level (i.e., systolic array-level). Consequently, shrinking the associated configuration overheads (discussed in Section III-D).

Equation 3 expresses the size of reduced design space (Ω_c) obtained after constraining the variables BW, K, N, and L.

$$|\Omega_c| = \sum_{N=2,3,4} \sum_{L=1}^N \binom{N^2}{L} \quad (3)$$

Using numerical methods, we evaluate $|\Omega_c|$ to be 66062. For a DNN with n layers, $|\Omega_c| = 66062^n$. This is a large size for practical design space exploration, especially since re-training is needed to alleviate the accuracy degradation caused by approximation. Motivated by this, we prune Ω by eliminating the sub-optimal Ax-BxP configurations.

3) *Design Space Pruning*: We prune the search space by restricting the contents of the set Π_{Ax} for a given L. Figure 5 illustrates the possible choices of Π_{Ax} , wherein W_{BxP} and A_{BxP} are the Ax-BxP weight and activation tensors, respectively, of a DNN layer. Further, \tilde{N}_W (\tilde{N}_A) and \mathcal{I}_W (\mathcal{I}_A) represent number of blocks and block indices respectively, of W_{BxP} (A_{BxP}) used for computing the MAC operation ($W_{BxP} * A_{BxP}$). As shown, there are a variety of ways of choosing 4 (L) out of 16 (N^2) partial products. The selected partial products (shown in green) cast a shape on the 2D array that represents all possible N^2 partial products. The shape could be scattered, irregular, or regular. In our design exploration, we restrict to regular shapes that substantially reduces the search space complexity. Formally, restricting to regular shapes constraints L as shown in Equation 4.

$$L = \tilde{N}_W * \tilde{N}_A. \quad (4)$$

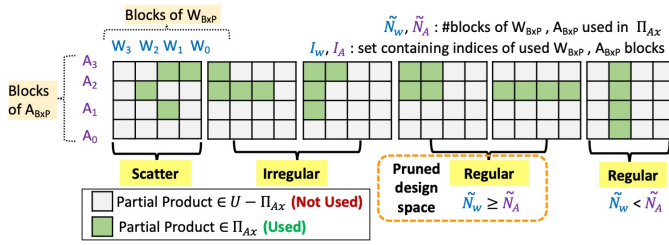


Fig. 5: Design search space for L=4, N=4: Illustration

Based on previous studies that show activations to be more sensitive to precision-scaling than weights during DNN inference operations [19], [10], we further prune the search space such that $\tilde{N}_A \geq \tilde{N}_W$. In other words, we never select configurations (e.g., the right most configuration in Figure 5), wherein a weight operand (W_{BxP}) has more blocks than an activation operand (A_{BxP}). Equation 5 show the size of the design search space (Ω_{c+p}) obtained after pruning, wherein $\binom{N}{\tilde{N}_W}$ and $\binom{N}{\tilde{N}_A}$ are the number of possible ways of

selecting \tilde{N}_W and \tilde{N}_A blocks, respectively, out of N blocks. It is worth mentioning that although Equation 5 restricts the number of choices of Π_{Ax} , it enables an efficient systolic array implementation so that we can retain the benefits achieved using Ax-BxP at system-level due to reduced computation, memory footprint and memory traffic.

$$|\Omega_{c+p}| = \sum_{N=2,3,4} \sum_{\tilde{N}_W=1}^N \sum_{\tilde{N}_A=1}^{\tilde{N}_W} \binom{N}{\tilde{N}_W} \binom{N}{\tilde{N}_A} \quad (5)$$

4) *Design heuristics*: Next, we present the two heuristics, viz., *static-idx* and *dynamic-idx*, that are used for performing $\binom{N}{\tilde{N}_W}$ and $\binom{N}{\tilde{N}_A}$ functions (i.e., selecting \tilde{N}_W blocks of W_{BxP} and \tilde{N}_A blocks of A_{BxP}).

In the *static-idx* heuristic, the operand blocks are chosen in a *significance-aware* manner where the blocks of higher significance are always chosen over the blocks of lower significance. For a given \tilde{N} , we first find the index of the most-significant non-zero block of the operand tensor and

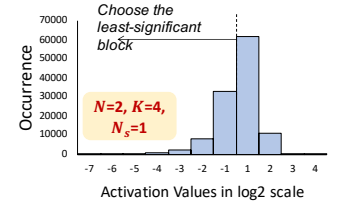


Fig. 6: Significance of the non-zero activation blocks in a layer of quantized AlexNet

choose the next \tilde{N} consecutive blocks in the decreasing order of significance. Since the blocks of data in the *data* field of the Ax-BxP tensor are arranged in the decreasing order of significance by default, we require only the start index ($\mathcal{I}[N-1]$) or the end index ($\mathcal{I}[0]$) to determine the indices of all the blocks. Recall that \mathcal{I} is common to all the scalar elements of an operand tensor. When \mathcal{I} is chosen using the *static-idx* heuristic, it only contains the index of the most significant block. For instance, consider the activation histogram (generated using ImageNet dataset) of a quantized AlexNet layer shown in Figure 6, where the activation values are represented using 2 blocks of 4 bits each, (i.e $N = 2, K = 4$). In the histogram, both blocks may be non-zero for large values that reside in bins [1,3], whereas only the least significant block is non-zero for the values in bins [-4,-1]. Therefore, when $\tilde{N} = 1$, *static-idx* heuristic chooses the most significant block covering values in bins [1,3] and approximating the small values in bins [-4,-1] to zero.

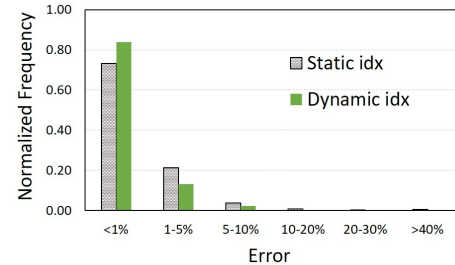


Fig. 7: Operand blocks selection heuristics: Error Analysis

Next, we introduce *dynamic-idx* heuristic, where the set \mathcal{I} is chosen specifically for each scalar element in a tensor and the smaller values could also be represented with high resolution.

TABLE I: Design Space for approximate blocked computation

Block-size	Ax-BxP configuration = $\{(K, \tilde{N}_W, \tilde{N}_A)\}$
$K = 2$	$\{(2,1,4), (2,1,3), (2,2,2), (2,1,2), (2,1,1)\}$
$K = 3$	$\{(3,1,3), (3,1,2), (3,1,1)\}$
$K = 4$	$\{(4,1,2), (4,1,1)\}$

In the *dynamic-idx* heuristic, the distribution of the scalar values (of a tensor) in different blocks is used in determining the set \mathcal{I} (i.e., the index of the most significant block). Subsequently, each scalar is represented using \tilde{N} consecutive blocks starting from it's most-significant non-zero block. Note that the dynamic choice heuristic is based on both significance and value of the blocks. Figure 7 quantifies the advantage of *dynamic-idx* heuristic over the *static-idx* by showing the obtained error distribution (obtained using ImageNet dataset) on an Alexnet layer. As shown, *dynamic-idx* can achieve much lower error rate in comparison to *static-idx* heuristic. It is worth mentioning that the block indices in the set \mathcal{I} could be chosen in a non-contiguous manner. However, we observe that adopting non-contiguous blocks show no advantage in representing DNN data-structures and can lead to considerable control logic overhead. Further, as previously mentioned, when contiguous blocks are chosen, $|\mathcal{I}| = 1$, as we just need to store the index of the most significant block. Memory saving is less for *dynamic-idx* heuristic in comparison to *static-idx* heuristic, as we need to store \mathcal{I} for each scalar. For a given N and \tilde{N} , the overhead of appending \mathcal{I} to each data element is $\lceil \log_2((N - \tilde{N}) + 1) \rceil$ bits. For example, if $K=2$, $N=4$, $\tilde{N}=2$, we have 2 additional bits (for index in \mathcal{I}) every 4 ($K \cdot \tilde{N}$) compute bits. Therefore, the overall memory footprint decreased by $\sim 25\%$ (from 8 bits to 6 bits).

Since L and the set Π_{Ax} can be derived for a given K , \tilde{N}_W and \tilde{N}_A , the design space Ω can now be re-characterized as a set of all 3-tuples $\{K, \tilde{N}_W, \tilde{N}_A\}$ that satisfy all the constraints discussed thus far. The Ax-BxP configurations in Ω are listed against the block-size K in Table I. Furthermore, we define two modes of Ax-BxP *Static* and *Dynamic* where the operand blocks are chosen using the *static-idx* heuristic and the *dynamic-idx* heuristic respectively.

5) *Designing DNNs using Ax-BxP*: We now present a systematic methodology to design DNNs using Ax-BxP. Algorithm 1 describes the pseudo code that we utilize to identify best Ax-BxP configuration for each data-structure of each DNN layer. It takes a pre-trained DNN model (DNN_{Fxp}), a training dataset (Tr_{data}), a target block size (K_{tgt}), and a limit on allowed accuracy degradation (γ) as inputs and produces Ax-BxP DNN (DNN_{AxBxP}) as an output. We first utilize Tr_{data} to evaluate the baseline network accuracy (line 2) and construct data-value histograms ($DsHist_{list}$) of each data-structure within the network (line 3). Next, we identify the best Ax-BxP configuration for a DNN layer using the histograms of the associated weight (W_{Fxp}) and activation (A_{Fxp}) pair (lines 4-10). As detailed in Algorithm 1, to obtain best Ax-BxP configuration, we first form a pruned search space (Ω_{c+p}) (line 5), and subsequently, explore the choices within Ω_{c+p} to find the best Ax-BxP configuration which is represented by \tilde{N}_W , \tilde{N}_W , N_A , and \tilde{N}_A (line 6). Next, data-structures are converted to Ax-BxP tensor using the Convert-To-AxBxP

function (lines 7-8) and inserted into DNN_{AxBxP} network (line 9). Once all data-structures are converted to Ax-BxP tensor, we re-train DNN_{AxBxP} until the network accuracy is within the desired degradation limit ($< \gamma$) or the maximum allowed trained epochs (maxEpoch) is exceeded.

Algorithm 1: Designing AxBxP DNN

Input: DNN_{Fxp} : Pre-trained FxP DNN, Tr_{data} : Training dataset, γ : Max Accuracy Loss, K_{tgt} : Target block size
Output: DNN_{AxBxP} : Approximate Blocked DNN

- 1: $DNN_{AxBxP} = DNN_{Fxp}$ /* initialize */
- 2: $Acc_{Fxp} = \text{computeAccuracy}(DNN_{Fxp})$
- 3: $DsHist_{list} = \text{getDist}(DNN_{Fxp}, Tr_{data}) \forall$ datastructures
- 4: **for each** [Weight (W_{Fxp}), Activations (A_{Fxp})] pair $\in DsHist_{list}$
- 5: $\Omega_{c+p} = \text{formPrunedSearchSpace}(W_{Fxp}, A_{Fxp}, K_{tgt})$ /* Searching best AxBxP configuration */
- 6: $(\tilde{N}_W, \tilde{N}_W, N_A, \tilde{N}_A) = \text{getBestConfig}(\Omega_{c+p})$
- 7: $W_{AxFxp} = \text{Convert-To-AxBxP}(W_{Fxp}, \tilde{N}_W, \tilde{N}_W, K_{tgt})$
- 8: $A_{AxFxp} = \text{Convert-To-AxBxP}(A_{Fxp}, N_A, \tilde{N}_A, K_{tgt})$
- 9: insert-AxBxP-Tensors ($DNN_{AxBxP}, W_{AxFxp}, A_{AxFxp}$)
- 10: **end for**
- 11: numEpochs=0/* Re-train */
- 12: **while** $\gamma < (Acc_{Fxp} - \text{computeAccuracy}(DNN_{AxBxP}))$ **and** numEpochs $<$ maxEpoch)
- 13: Ax-BxP-Aware-Training (DNN_{AxBxP}, Tr_{data})
- 14: numEpochs++
- 15: return DNN_{AxBxP}

Algorithm 2: Convert-To-AxBxP

Input: X_{Fxp} : FxP tensor, (K, N_X, \tilde{N}_X) : Ax-BxP configuration
Output: X_{AxFxp} : Ax-BxP tensor

- 1: **For each** scalar x in X_{Fxp}
- 2: $Block_{list} = \text{Get-Significance-Sorted-Blocks}(x, K, N_X)$
- 3: $\mathcal{I}_x = \text{get-idx-first-Non-Zero-block}(Block_{list})$
- 4: $X_{AxFxp} = \text{pick-insert-Blocks-in-Range}(\mathcal{I}_x, \mathcal{I}_x \cdot \tilde{N}_X)$
- 5: return X_{AxBxP}

Algorithm 2 outlines the pseudo code for converting FxP tensors to Ax-BxP tensors using dynamic-idx heuristic. It takes an FxP tensor (X_{Fxp}) and Ax-BxP configuration (K, N_X, \tilde{N}_X) as inputs and produces an Ax-BxP tensor (X_{AxFxp}) as output. A key function of this algorithm is to determine indexes (\mathcal{I}_x) of the chosen blocks. To achieve this objective, we first convert fixed point scalars to blocked fixed-point scalars (line 2) and subsequently, pick \tilde{N}_X contiguous blocks starting from the first non-zero block. Next, the chosen blocks and indexes are inserted into the Ax-BxP tensor (line 4). After all scalars have been converted X_{AxFxp} tensor is returned (line5).

D. Ax-BxP DNN Accelerator

We present the Ax-BxP DNN Accelerator that can support Ax-BxP. This accelerator is designed through simple enhancements to a conventional systolic array based DNN accelerator such as AxBxP PE, control logic and ToAxBxP logic. For a given $K \in \Omega_{c+p}$ and a given mode of Ax-BxP (i.e static or dynamic), our proposed AxBxP PE can support all the Ax-BxP configurations using the control logic.

To demonstrate how inference is realized using Ax-BxP accelerator, we consider the MAC operations in a layer of DNN, where W and A are the weight and activation tensors, respectively, represented in the Ax-BxP format. The Ax-BxP accelerator is illustrated in Figure (8), where dedicated control blocks which share the same control logic, are placed to process the input data in each row and column of the systolic array. The control blocks generate the operands and shift amounts for the multipliers and shifters, respectively of the AxBxP PEs to perform approximate MAC computations and produce the output activations. The output activations are converted to Ax-BxP format by the *ToAxBxP* logic, using the methodology described in Algorithm 2. Let us now discuss the design of the *AxBxP PE* and the *Control* logic in detail.

1) *Ax-BxP Processing Element (AxBxP PE)*: AxBxP PEs perform Ax-BxP MAC operations using the operands and shift amounts generated by the control logic. During each cycle, the control logic generates N operand blocks and the corresponding shift amounts. In a given Ax-BxP PE, for $m = 0, \dots, N - 1$, the m^{th} signed multiplier generates the partial product $op_W[m] * op_A[m]$ which is shifted by a shift amount of $(s_a[m] + s_w[m])$ in the m^{th} shifter. The shifted partial products are added using an adder-tree to generate the approximate product. The approximate products generated in each cycle are then accumulated in the accumulator. It is worth noting that as L decreases, the throughput achieved by Ax-BxP PEs increases, since a fixed number (N) of multiplications are performed in each cycle.

For a given K and a given mode of Ax-BxP, Ax-BxP PEs support all the Ax-BxP configurations in Ω_{c+p} with block size K by allowing shifts by different amounts. The different shift amounts are realized in the shifters using multiplexers. The number of multiplexers increases with the number of unique shift amounts to be supported, resulting in increases in energy and area overheads. It is straightforward to show that larger number of unique shift amounts must be supported by the Ax-BxP PE during dynamic Ax-BxP compared to static Ax-BxP. Therefore, the energy and area of Ax-BxP PEs are comparatively lower during the static mode.

2) *Control*: The control logic blocks in the Ax-BxP accelerator partition $data_A$ and $data_W$ into blocks of K bits each, and determine the shift amounts corresponding to each of these blocks. The shift amounts are determined based on the values $K, N, \tilde{N}_A, \mathcal{I}_A, \tilde{N}_W$ and \mathcal{I}_W , which are broadcast to the control blocks at the start of a layer's computations.

To elaborate on the control logic, let us consider the control block in a given row of the systolic array. Note that the control block in a given column functions analogously. For a given input of the i^{th} element $data_A[i]$ in $data_A$, the control logic generates the operand blocks $op_A[j] = data_A[i, j]$, where

$j = 0, \dots, \tilde{N}_A - 1$ by first partitioning $data_A[i]$ into \tilde{N}_A blocks of K bits each, and then sign extending each of these blocks by 1-bit, based on the sign bit of $data_A[i]$. During static mode, the shift amount corresponding to $data_A[i, j]$ is $(\mathcal{I}_A + j) * K$. During dynamic mode, this singleton is determined individually for each $data_A[i]$ in $data_A$, which we denote as $\mathcal{I}_A[i]$ to emphasize the dependency on $data_A[i]$. Therefore, the shift amount corresponding to the j^{th} block $data_A[i, j]$ is $(\mathcal{I}_A[i] + j) * K$.

Thus far, for a given $data_A[i]$, we have shown how to generate the values of \tilde{N}_A out of N operand blocks and the corresponding shift amounts. When $L = \tilde{N}_W * \tilde{N}_A = N$, the remaining $N - \tilde{N}_A$ values are obtained by simply replicating the \tilde{N}_A operand blocks and shift amounts. That is,

```

for  $i = 0 : \tilde{N}_W - 1$  do
  for  $j = 0 : \tilde{N}_A - 1$  do
     $op_A[i * \tilde{N}_A + j] = op_A[j]$ 
     $s_a[i * \tilde{N}_A + j] = s_a[j]$ 
  end for
end for

```

When $L < N$, subsequent elements of $data_A$ are used such that N operand blocks and shift amounts are generated in each cycle. Furthermore, it is worth noting that the design complexity of both the Ax-BxP PEs and the control logic depends on the number of unique shift amounts to be supported which in-turn depends on L . Therefore, constraining L to be $\leq N$ minimizes the design complexity while preserving the classification accuracy (as shown in section V).

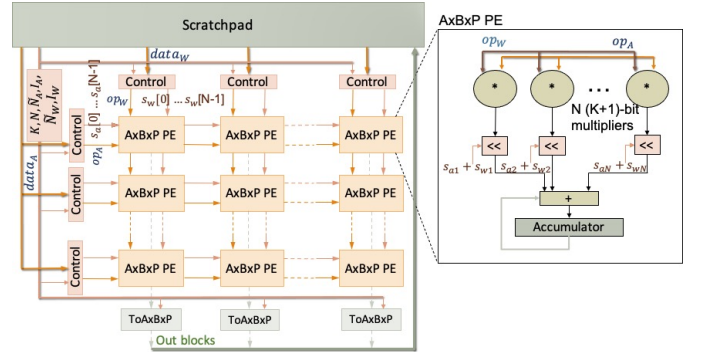


Fig. 8: Ax-BxP Accelerator

IV. EXPERIMENTAL METHODOLOGY

In this section, we present our experimental methodology for evaluating Ax-BxP.

Accuracy Evaluation: We evaluate our proposed Ax-BxP using state-of-the-art image recognition DNNs for the ImageNet and CIFAR10 dataset, *viz.* ResNet50, MobileNetV2 and AlexNet. We obtain the precision configurations for mixed-precision evaluation on ResNet50 and MobileNetV2 from the previous works, PACT[10] and HAQ[7].

System Energy and Performance Evaluation: We design our proposed Ax-BxP DNN accelerator by expanding the conventional systolic array accelerator modelled in ScaleSim [20] using enhancements such as Control logic, ToAxBxP logic and the Ax-BxP PEs, all synthesized to 15nm technology

node using Synopsis Design Compiler. We consider a systolic array of size 32×32 and on-chip memory of size 2MB. On-chip memory is modelled using CACTI [21]. We design our baseline FxP8 accelerator, also synthesized to 15nm technology node using Synopsis Design Compiler, as a conventional systolic array with FxP8 PEs that can implement 8-bit MAC operations. The system-level energy and performance benefits of the Ax-BxP accelerator are evaluated against the FxP8 accelerator at iso-area. Furthermore, we use the Bit-Fusion accelerator [17] to demonstrate the energy and performance benefits of Ax-BxP over exact computations.

V. RESULTS

In this section, we demonstrate the energy and performance benefits of using Ax-BxP w.r.t exact computations at the cost of small accuracy degradation due to the approximations. Furthermore, we demonstrate the benefits of Ax-BxP w.r.t exact computations in the Bit-Fusion accelerator.

A. PE-level Energy and Area Benefits

Figure 9 shows the energy and area benefits of AxBxP PE for $K = 2, 3, 4$, and Bit-Fusion PE w.r.t FxP8 PE. On an average, the energy and area benefits of AxBxP PE in dynamic mode are $1.87x$ and $1.12x$, respectively. In static mode, the average energy and area benefits are $1.95x$ and $1.32x$, respectively.

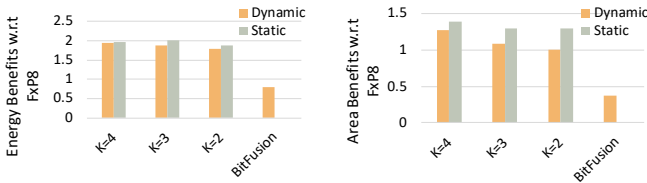


Fig. 9: Computation Energy and Area Benefits w.r.t. FxP8 baseline

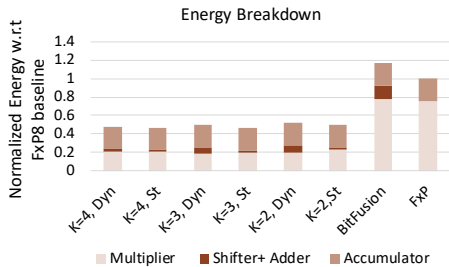


Fig. 10: Computation Energy Breakdown w.r.t. FxP8 baseline

Recall from section III-D that for a given K , the AxBxP PEs can support any Ax-BxP configuration by allowing shifts by different amounts. Additionally, the energy and area overheads of AxBxP PEs increase with an increase in the number of unique shift amounts to be supported. The number of unique shift amounts to be supported are proportional to N . Since the block-size K is inversely proportional to N , the energy benefits decrease as K decreases during both static and dynamic Ax-BxP. Furthermore, since greater number of shift amounts are to be supported for the dynamic mode, the

TABLE II: Best Dynamic Ax-BxP configurations

Block-size	AlexNet	ResNet50	MobileNetV2
$K = 4$	(4,1,1)	(4,1,2)	(4,1,2)
$K = 3$	(3,1,1)	(3,1,2)	(3,1,2)
$K = 2$	(2,1,2)	(2,1,2)	(2,2,2)

energy benefits during dynamic Ax-BxP are lower than static Ax-BxP for all K . Figure 10 shows the energy breakdown of multipliers, shifters and adders, and the accumulator in AxBxP PEs for all K in both static and dynamic modes of Ax-BxP. For approximately equal multiplier and accumulator energy, we observe that the overhead due to re-configurability (i.e shifters and adders) is greater in dynamic mode vs static mode.

Furthermore, we observe that the Bit-Fusion PE exhibits significant energy and area overheads compared to AxBxP PEs. This is because, the Bit-Fusion PE is composed of 16 bit-bricks that can perform 3-bit signed MAC. All the 16 bit bricks are used to perform 8-bit MAC. Compared to this, AxBxP PE with $K = 2$ can perform 8-bit MAC using only 4 3-bit signed multiplications. Also, the number of unique shift amounts supported by AxBxP PEs are smaller than the Bit-Fusion PE. Figure 10 shows the significantly lower multiplier energy, and the shifter and adder energy of the AxBxP PEs compared to the Bit-Fusion PE.

B. System Benefits and ImageNet Accuracy of dynamic Ax-BxP with varying config. across DNNs

1) *Energy Benefits*: Figure 11 shows the system-level energy benefits of dynamic Ax-BxP inference compared to an FxP8 baseline. We perform the inference using ImageNet dataset with state-of-the-art DNNs such as AlexNet, ResNet50 and MobileNetV2. We find that the best Ax-BxP configuration in Ω_{c+p} for a given K , i.e the configuration that provides maximum energy benefits with minimum accuracy loss ($< 1\%$), varies across the networks considered. For a given network, we maintain the Ax-BxP configurations uniform across its layers.

Table II shows the best Ax-BxP configuration for a given K and network. The proposed Ax-BxP DNN accelerator efficiently supports varying Ax-BxP configurations across networks and achieves system-level energy benefits of $1.11x$ - $1.91x$, $1.11x$ - $1.88x$ and $1.19x$ - $1.72x$ for $K = 4, 3$ and 2 , respectively.

Figure 11 shows that for a given K , when L decreases, the energy benefits increases. This is because the throughput of the Ax-BxP DNN accelerator increases when L decreases as discussed in section III-D. Therefore, the overall inference cycles reduces, resulting in superior energy benefits. On the other hand, the classification accuracy decreases with a decrease in L .

Furthermore, for a given L , the energy benefits increases as K decreases. This is because the memory footprint, number of off-chip accesses and the computational energy is lower for smaller K . However, the classification accuracy decreases since the overall precision (number of bits) of operands decreases. It is worth noting that when $L < N$ during dynamic Ax-BxP, the memory-footprint savings are affected by storing the $\lceil \log_2((N - \tilde{N}) + 1) \rceil$ bits of operand block indices. Despite

this, since the throughput is increased for smaller L , we observe significant energy benefits.

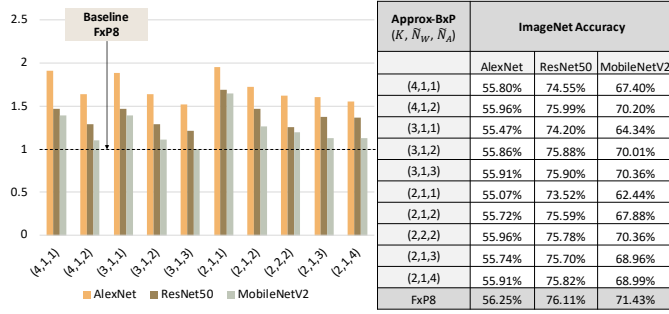


Fig. 11: System-level Energy Benefits with dynamic Ax-BxP

2) *Performance Benefits*: The performance benefits during dynamic Ax-BxP w.r.t FxP8 at iso-area are shown in Figure 12. We obtain 1.29x-2.66x, 1.1x-2.9x and 1.02x-4.1x performance benefits for $K = 4, 3$ and 2, respectively. For a given K , smaller L results in increased throughput which results in increased performance. Furthermore, for a given L , lower K results in lower area of Ax-BxP PEs. Therefore, larger number of PEs can be used at iso-area, which results in reduced number of cycles.

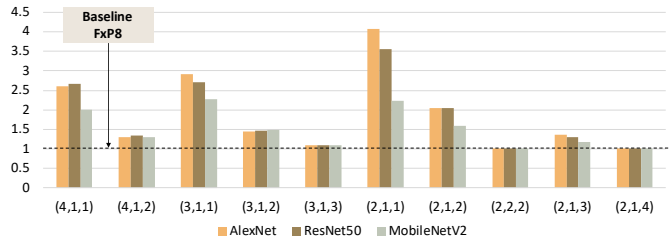


Fig. 12: System-level Performance Benefits with dynamic Ax-BxP

C. System-level Energy Benefits and ImageNet Accuracy with varying Ax-BxP configurations within DNNs

1) *Energy Benefits*: The benefits of Ax-BxP can be further highlighted in the context of variable-precision DNNs that have different layer-wise precision requirements. The precision configurations considered are shown in Figure 13, where we vary the precision in a coarse-grained manner across the layers in units of 4-bits. We perform dynamic Ax-BxP with a combination of the configurations (4, 1, 1) and (4, 2, 1) across layers. Here, the classification accuracy is evaluated with the ImageNet dataset.

We achieve 1.2x system-level energy benefits in AlexNet with negligible loss in classification accuracy. We consider two different precision configurations from previous works such as PACT[10] and HAQ[7] to evaluate the variable-precision energy benefits with ResNet50 and MobileNetV2.

The PACT configuration restricts the precision of weights and activations of all layers to 3-bits, except the first and last layer, which are set to 8 bits. Due to this aggressive quantization, minor accuracy degradation is reported in PACT, which is replicated in our results in Figure 13. Using our proposed hardware, we achieve 2.39x system-level energy improvements for ResNet50 by adopting the PACT configuration.

The HAQ configuration sets the precision of weights and activations in the range of 3 to 8, across layers. We fine-tune this configuration to implement dynamic Ax-BxP with $K = 4$, across layers. With the finetuned HAQ configuration for ResNet50 and MobileNetV2, we observe that the minor accuracy degradation caused by aggressive quantization using PACT is alleviated at the cost of somewhat lower energy benefits. We achieve a system-energy improvement of 1.36x and 1.14x with ResNet50 and MobileNetV2 respectively.

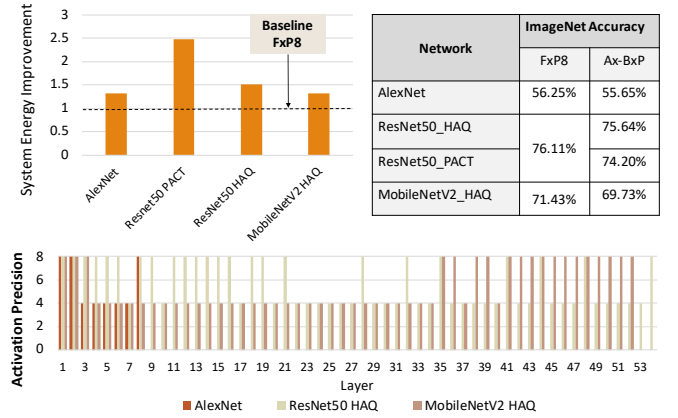


Fig. 13: System-level Energy benefits and ImageNet accuracy for mixed-precision networks

2) *Performance Benefits*: Figure 14 shows the system-level performance benefits of using Ax-BxP for mixed-precision networks. Using PACT configuration we obtain 3.62x performance benefits for ResNet50. Since we use the Ax-BxP configuration of (2,1,1) for all layers except the first and the last layers, we achieve maximum throughput resulting in significantly high performance benefits. Using the HAQ configuration, we minimally sacrifice the performance benefits to achieve superior accuracy.

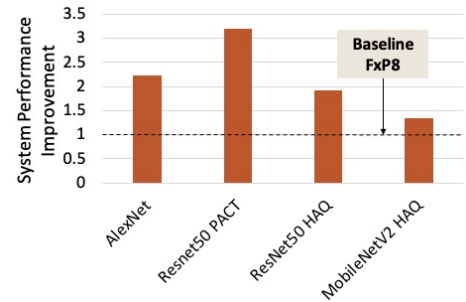


Fig. 14: System-level Performance benefits and ImageNet accuracy for mixed-precision networks

D. Benefits of Ax-BxP in the Bit-Fusion Accelerator

The energy and performance benefits of dynamic Ax-BxP in the Bit-Fusion accelerator with respect to exact computations, is shown in Figure 15. We have considered the Ax-BxP configurations with $K = 2$, since the bit-bricks in Bit-Fusion PE are designed for a block-size of 2. By performing approximations using Ax-BxP, we could achieve energy benefits upto 1.51x

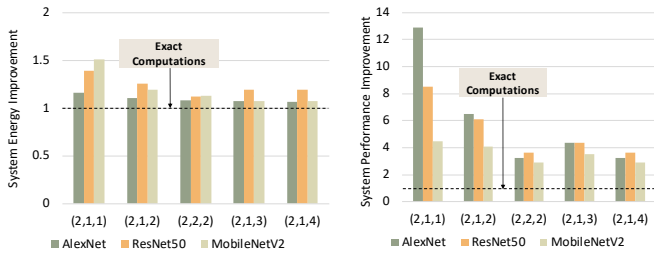


Fig. 15: Ax-BxP Benefits in BitFusion

and performance benefits upto 12.87x in the Bit-Fusion accelerator. The Bit-Fusion PEs achieve a comparatively higher throughput for a given L . The increase in throughput is as high as 16x when $L = 1$, resulting in 12.5x benefits for the configuration (2, 1, 1).

E. System Benefits and ImageNet Accuracy of static Ax-BxP with varying config. across DNNs

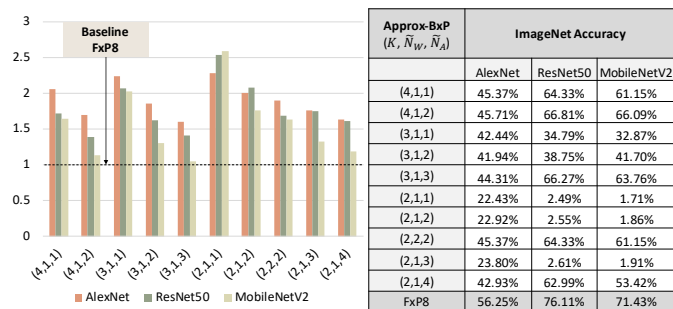


Fig. 16: System-level Energy Benefits with static Ax-BxP

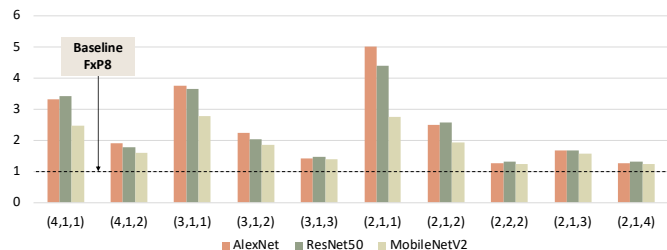


Fig. 17: System-level Performance Benefits with static Ax-BxP

Figure 16 shows the energy benefits of static Ax-BxP. The benefits during static Ax-BxP are greater than the dynamic Ax-BxP across networks and across configurations. This is because the Ax-BxP PEs are simpler in terms of the number of shift amounts to be supported during the static mode, compared to the dynamic mode. Furthermore, the memory footprint of the operands are lower during static mode compared to the dynamic mode, since the cost of storing and fetching \mathcal{I}_W and \mathcal{I}_A are amortized across the tensors W and A , respectively. As a result the memory access energy is lower and the compute energy is lower during static Ax-BxP. However, the ImageNet accuracy degradation with static Ax-BxP is significantly higher than dynamic Ax-BxP across configurations and networks. The performance benefits with static Ax-BxP are shown in Figure 17. The performance benefits during static Ax-BxP is greater than dynamic Ax-BxP

across networks and Ax-BxP configurations. This is because in static mode, the Ax-BxP PEs exhibit significant area benefits, which is exploited to achieve higher throughput.

VI. RELATED WORK

The computation and storage demands posed by DNNs has motivated several efforts to focus on model quantization, or precision scaling. While some of the early efforts that proposed simple quantization techniques are effective in small networks, they suffer significant accuracy degradation in large networks [22], [23], [19], [24], [25].

More recent efforts have developed advanced quantization techniques and training methodologies that work well for a wide range of networks and effectively reduce the bit-widths of data-structures to below 8 bits. Notably, PACT [10] has demonstrated successful inference using only 2-bit precision for weights and activations, except for the first and last layers, which are evaluated at 8-bit precision. Other efforts such as BQ [9] and WRPN [8] also achieve adequate inference accuracy using 2-bit weights and activations, by using techniques such as Balanced Quantization and Model scaling respectively. Deep Compression [26] employs model pruning, trained quantization and Huffman coding to reduce the model size. Bi-Scaled DNN [11] and Compensated DNN [27] leverage the value statistics in DNNs and design number-formats and error compensation schemes that effectively reduce the overall bit-width.

Although these efforts enable DNN inference with ultra-low (below 8-bit) precision, a common precision is not optimal across networks or even across layers within a network. For example, it is a common practice to retain the first and last layers at high precision while quantizing other layers to very low precision in order to preserve accuracy. This fact is further emphasized by works like HAQ [7], which argue that the minimum precision requirement varies within a network, across different layers.

Since varying precision requirements are inherent across DNNs, several efforts [14], [15], [17] have focused on the design of precision re-configurable hardware. BISMO [14] proposes a parallelized bit-serial architecture that offers maximum flexibility in terms of bit-widths it can support. Stripes [15] is a similar work that uses bit-serial hardware design to support variable precision. Albeit offering maximum flexibility, the performance of bit serial hardware is limited by high latency and energy caused by its serial nature. In contrast, fixed-precision hardware needs to be designed to support maximum precision and hence is over-designed for applications with low precision requirement. Instead of performing computations serially at the granularity of bits, BitFusion [17] explores serial computation at the granularity of a group of bits and demonstrates superior energy benefits compared to state-of-the-art bit-serial and fixed-precision accelerators. None of these efforts explore the use of approximations to improve the efficiency of variable-precision hardware. Exploiting the resilience of DNNs to approximations, we propose approximate blocked computation as a next step that is complementary to previous efforts. Computations are performed block-wise, where blocks are a group of bits of fixed length. Our

approximation methodology reduces the number of block-wise computations, while maintaining the inference accuracy.

The design of approximate multipliers has been extensively explored in the literature. These efforts can be broadly classified into three categories – efforts that focus on the design of general-purpose approximate circuits, efforts that approximate partial-product accumulation, and efforts that approximate partial product generation.

General-purpose approximate circuits are designed by voltage over-scaling (VOS)[28] i.e reducing the supply voltage beyond the nominal value and logic simplification[29], [30]. In [28], since VOS most commonly affects the higher-order bits, this technique causes significantly high computational errors that cannot be easily corrected. Efforts such as [29] and [30] automatically design approximate circuits by reducing the logic-complexity for a given error constraint. The modelling and analysis tool [31] enables systematic evaluation of approximate circuits to choose between different approximate implementations. The greedy logic simplification approach used in these methods systematically eliminates circuit components based on the circuit activity profile. A more energy-efficient way to eliminate multiplier circuit components is by systematically minimizing the computation and accumulation of partial products.

Energy reduction during partial product accumulation can be achieved by approximate adders [32], [33], [34] or by approximate accumulation techniques [35]. While these efforts focus on minimizing the energy consumption of accumulation, we note that the multipliers are the primary sources of energy consumption during MAC operations. Several previous works [36], [37], [38], [39], [40], [41] have explored the approximation of partial product generation.

In [36], the authors propose a 2×2 under-designed multiplier block and build arbitrarily large power efficient in-accurate multipliers. The inaccurate 4:2 counter in [37] can effectively reduce the partial product stages of the Wallace multiplier. In [38], the authors substitute multiplication with additions and shift operations by representing the integer operands as logarithms with an error correction factor. The computation sharing multiplier proposed in [39], [40] specifically targets computation re-use in vector-scalar products. Reference [41] proposes an approximate multiplier that performs approximation on only the multiplication of lower-order bits. These efforts achieve only computational energy benefits. In contrast, since our proposed Ax-BxP method minimizes the number of operand blocks used in computation, we achieve savings in terms of memory footprint and memory traffic in addition to computational energy savings. Other efforts such as [42], [43], [44], [45], [46], [47] have taken a similar approach.

Operand bit-width truncation to minimize partial product generation is explored by efforts such as [42], [43] and [44]. However, these efforts exhibit poor performance during small bit-width computations. In [45], the authors extract an m -bit segment from an n -bit operand and perform an m -bit ($m;n$) bit multiplication, achieving significant energy benefits. However the segments must be at least $n/2$ bits long, thus limiting the energy savings. An improvement over [45] is proposed by [46] that reduces the segment size beyond $n/2$ while minimizing

error, enabling dynamic range multiplication. However, this approach involves extra complex-circuitry such as leading one-bit detectors, barrel shifters etc., which introduces considerable delay, area and energy overheads that decrease the approximation benefits. The partial product perforation method proposed by [47] aims at generating fewer partial products by dropping a few bits of one operand during multiplication. Since this approach reduces the bit-width (precision) of just one operand, it does not fully utilize the benefits of precision scaling. Moreover, it requires complex error correction methods that further limit the benefits of approximation method. Additionally, none of the efforts discussed thus far support variable precision computations which we have explored in our work. Reference [48] proposes dynamic range floating-point (FP) format. However, the area and power cost of supporting FP computations is much higher than fixed-point (FxP) computations. In [27], the authors propose error-compensation techniques for reduced-precision FxP multiplication. A novel number format to represent dual-precision FxP numbers is proposed in [11]. The proposed Ax-BxP format supports a wide range of precision requirement. It enables efficient re-configurability at block granularity while minimizing the approximation errors.

VII. CONCLUSION

The minimum bit-width requirement varies across and within DNNs to preserve classification accuracy. Optimally supporting such varying precision configurations in DNN accelerators is the challenge addressed by our work. We address this challenge algorithmically and in hardware using our proposed Approximate Blocked Computation method. We demonstrate the effectiveness of our approximation algorithm by exhibiting negligible loss in classification accuracy with ImageNet dataset in state-of-the art DNNs such as AlexNet, ResNet50 and MobileNetV2. Our proposed systolic-array based architecture that implements Ax-BxP, provides upto 1.34x and 1.6x benefits in system energy and performance respectively, with varying Ax-BxP configurations across networks. Further, with varying Ax-BxP configurations across layers within networks, we achieve upto 1.67x and 1.93x improvements in system energy and performance, respectively.

ACKNOWLEDGEMENT

This work was supported by C-BRIC, one of six centers in JUMP, a Semiconductor Research Corporation (SRC) program, sponsored by DARPA.

REFERENCES

- [1] J. X. Chen. The evolution of computing: Alphago. *Computing in Science Engineering*, 18(4):4–7, 2016.
- [2] Dario Amodei et al. T. Brown. Language models are few-shot learners. *ArXiv*, abs/2005.14165, 2020.
- [3] Mingxing Tan and Quoc V. Le. Efficientnet: Rethinking model scaling for convolutional neural networks. 2019.
- [4] S. Venkataramani, K. Roy, and A. Raghunathan. Efficient embedded learning for iot devices. In *Asia and South Pacific Design Automation Conference (ASP-DAC)*, pages 308–311, Jan 2016.
- [5] V. Sze, Y. Chen, T. Yang, and J. S. Emer. Efficient processing of deep neural networks: A tutorial and survey. *Proceedings of the IEEE*, 105(12):2295–2329, Dec 2017.

- [6] N. P. Jouppi et al. In-datacenter performance analysis of a tensor processing unit. 2017.
- [7] K. Wang et al. Haq: Hardware-aware automated quantization with mixed precision. In *Proc. CVPR*, 2019.
- [8] A. Mishra et al. Wrpn: wide reduced-precision networks. *arXiv preprint arXiv:1709.01134*, 2017.
- [9] S. Zhou et al. Balanced quantization: An effective and efficient approach to quantized neural networks. *JCST*, 32(4), 2017.
- [10] J. Choi et al. Pact: Parameterized clipping activation for quantized neural networks. *arXiv preprint arXiv:1805.06085*, 2018.
- [11] S. Jain et al. Biscoled-dnn: Quantizing long-tailed datastructures with two scale factors for deep neural networks. In *Proc. DAC*. ACM, 2019.
- [12] P. Judd et al. Proteus: Exploiting numerical precision variability in deep neural networks. In *In Proc. ICS*, 2016.
- [13] S. Hashemi et al. Understanding the impact of precision quantization on the accuracy and energy of neural networks. *CoRR*, abs/1612.03940, 2016.
- [14] Y. Umuroglu et al. Bismo: A scalable bit-serial matrix multiplication overlay for reconfigurable computing. In *ICFPL*. IEEE, 2018.
- [15] P. Judd et al. Stripes: Bit-serial deep neural network computing. In *MICRO*. IEEE, 2016.
- [16] S. Sharify et al. Loom: Exploiting weight and activation precisions to accelerate convolutional neural networks. *CoRR*, abs/1706.07853, 2017.
- [17] H. Sharma et al. Bit fusion: Bit-level dynamically composable architecture for accelerating deep neural networks. In *Proc. ISCA*, 2018.
- [18] R. I. Hartley and K. K. Parhi. *Digit-Serial Computation*. 1995.
- [19] S. Zhou et al. Dorefa-net: Training low bitwidth convolutional neural networks with low bitwidth gradients. *arXiv preprint arXiv:1606.06160*, 2016.
- [20] A. Samajdar et al. Scale-sim: Systolic cnn accelerator. *arXiv preprint arXiv:1811.02883*, 2018.
- [21] N. Muralimanohar et al. Cacti 6.0: A tool to model large caches. *HP laboratories*, 27:28, 2009.
- [22] F. Li et al. Ternary weight networks. *arXiv preprint arXiv:1605.04711*, 2016.
- [23] I. Hubara et al. Quantized neural networks: Training neural networks with low precision weights and activations. *JMLR*, 18(1), 2017.
- [24] M. Courbariaux et al. Binarynet: Training deep neural networks with weights and activations constrained to +1 or -1. *arXiv preprint arXiv:1602.02830*, 2016.
- [25] M. Rastegari et al. Xnor-net: Imagenet classification using binary convolutional neural networks. In *ECCV*. Springer, 2016.
- [26] S. Han et al. Deep compression: Compressing deep neural networks with pruning, trained quantization and Huffman coding. *arXiv preprint arXiv:1510.00149*, 2015.
- [27] S. Jain et al. Compensated-dnn: energy efficient low-precision deep neural networks by compensating quantization errors. In *Proc. DAC*, 2018.
- [28] Y. Liu, T. Zhang, and K. K. Parhi. Computation error analysis in digital signal processing systems with overscaled supply voltage. *IEEE Transactions on Very Large Scale Integration (VLSI) Systems*, 18(4):517–526, 2010.
- [29] S. Venkataramani, A. Sabne, V. Kozhikkottu, K. Roy, and A. Raghunathan. Salsa: Systematic logic synthesis of approximate circuits. In *DAC Design Automation Conference 2012*, pages 796–801, 2012.
- [30] Z. Vasicek and L. Sekanina. Evolutionary approach to approximate digital circuits design. *IEEE Transactions on Evolutionary Computation*, 19(3):432–444, 2015.
- [31] R. Venkatesan, A. Agarwal, K. Roy, and A. Raghunathan. Macaco: Modeling and analysis of circuits for approximate computing. In *2011 IEEE/ACM International Conference on Computer-Aided Design (ICCAD)*, pages 667–673, 2011.
- [32] Ajay K. Verma, Phillip Brisk, and Paolo Jenne. Variable latency speculative addition: A new paradigm for arithmetic circuit design. In *Proceedings of the Conference on Design, Automation and Test in Europe*, page 1250–1255, 2008.
- [33] Ning Zhu, Wang Ling Goh, Weiya Zhang, Kiat Seng Yeo, and Zhi Hui Kong. Design of low-power high-speed truncation-error-tolerant adder and its application in digital signal processing. *IEEE Transactions on Very Large Scale Integration (VLSI) Systems*, 18(8), 2010.
- [34] V. Gupta, D. Mohapatra, S. P. Park, A. Raghunathan, and K. Roy. Impact: Imprecise adders for low-power approximate computing. In *IEEE/ACM International Symposium on Low Power Electronics and Design*, pages 409–414, 2011.
- [35] I. Qiqieh, R. Shafik, G. Tarawneh, D. Sokolov, and A. Yakovlev. Energy-efficient approximate multiplier design using bit significance-driven logic compression. In *Design, Automation Test in Europe Conference Exhibition (DATE), 2017*, pages 7–12, 2017.
- [36] P. Kulkarni, P. Gupta, and M. Ercegovac. Trading accuracy for power with an underdesigned multiplier architecture. In *2011 24th International Conference on VLSI Design*, pages 346–351, 2011.
- [37] C. Lin and I. Lin. High accuracy approximate multiplier with error correction. In *2013 IEEE 31st International Conference on Computer Design (ICCD)*, pages 33–38, 2013.
- [38] Patricio Bulić Uroš Lotrič. Applicability of approximate multipliers in hardware neural networks. *Neurocomputing*, 96:57–65, 2012.
- [39] Syed Shakib Sarwar, Swagath Venkataramani, Aayush Ankit, Anand Raghunathan, and Kaushik Roy. Energy-efficient neural computing with approximate multipliers. 14, 2018.
- [40] Jongsun Park, Hunsoo Choo, K. Muhammad, SeungHoon Choi, Yonghee Im, and Kaushik Roy. Non-adaptive and adaptive filter implementation based on sharing multiplication. In *2000 IEEE International Conference on Acoustics, Speech, and Signal Processing. Proceedings (Cat. No.00CH37100)*, volume 1, pages 460–463 vol.1, 2000.
- [41] Khaing Yin Kyaw, Wang Ling Goh, and Kiat Seng Yeo. Low-power high-speed multiplier for error-tolerant application. In *2000 IEEE International Conference of Electron Devices and Solid-State Circuits (EDSSC)*, pages 1–4, 2010.
- [42] M. J. Schulte and E. E. Swartzlander. Truncated multiplication with correction constant [for dsp]. In *Proceedings of IEEE Workshop on VLSI Signal Processing*, pages 388–396, 1993.
- [43] S. S. Kidambi, F. El-Guibaly, and A. Antoniou. Area-efficient multipliers for digital signal processing applications. *IEEE Transactions on Circuits and Systems II: Analog and Digital Signal Processing*, 43(2):90–95, 1996.
- [44] Jer Min Jou, Shiann Rong Kuang, and Ren Der Chen. Design of low-error fixed-width multipliers for dsp applications. *IEEE Transactions on Circuits and Systems II: Analog and Digital Signal Processing*, 46(6):836–842, 1999.
- [45] S. Narayanamoorthy, H. A. Moghaddam, Z. Liu, T. Park, and N. S. Kim. Energy-efficient approximate multiplication for digital signal processing and classification applications. *IEEE Transactions on Very Large Scale Integration (VLSI) Systems*, 23(6):1180–1184, 2015.
- [46] S. Hashemi, R. I. Bahar, and S. Reda. Drum: A dynamic range unbiased multiplier for approximate applications. In *2015 IEEE/ACM International Conference on Computer-Aided Design (ICCAD)*, pages 418–425, 2015.
- [47] G. Zervakis, K. Tsoumanis, S. Xydis, D. Soudris, and K. Pekmestzi. Design-efficient approximate multiplication circuits through partial product perforation. *IEEE Transactions on Very Large Scale Integration (VLSI) Systems*, 24(10):3105–3117, 2016.
- [48] J. Y. F. Tong, D. Nagle, and R. A. Rutenbar. Reducing power by optimizing the necessary precision/range of floating-point arithmetic. *IEEE Transactions on Very Large Scale Integration (VLSI) Systems*, 8(3):273–286, 2000.